Computer Assisted Methods in Engineering and Science
32(2): 155–177, 2025, https://doi.org/10.24423/cames.2025.1769

Optimal Bubble Deck Slabs with Respect to Ultimate and Serviceability Limit States

Natalia STASZAK[1)], Tomasz GAJEWSKI[2)], Tomasz GARBOWSKI[3)*]

[1)] *Doctoral School, Poznan University of Life Sciences, Poznan, Poland; e-mail: natalia.staszak@up.poznan.pl*

[2)] *Institute of Structural Analysis, Poznan University of Technology, Poznan, Poland; e-mail: tomasz.gajewski@put.poznan.pl*

[3)] *Department of Biosystems Engineering, Poznan University of Life Sciences, Poznan, Poland*

[*] *Corresponding Author e-mail: tomasz.garbowski@up.poznan.pl*

This article explores innovative approaches to the design of reinforced concrete bubble deck slabs. The primary objective is to achieve weight minimization while ensuring compliance with both ultimate limit state (ULS) and serviceability limit state (SLS) requirements. Advanced numerical homogenization techniques and a general nonlinear constitutive law (GNCL), within a finite element method (FEM) framework are employed to perform rapid and precise structural analysis. The study addresses the environmental impacts of traditional construction methods, emphasizing the need for sustainable design practices. By introducing voids into the structural elements of the deck slab, the research aims to reduce material consumption without compromising structural integrity. The optimization process involves identifying optimal design parameters, including the size of the bubble deck unit and the dimensions of the bubbles, to balance material efficiency and structural performance. Computational verification demonstrates that the proposed method accurately predicts displacements and stresses when compared to full 3D models. The results highlight the potential for significant material and cost savings, as well as a reduced environmental impact. The study concludes that the combination of numerical homogenization and GNCL offers a robust and flexible tool for the optimal design of reinforced concrete bubble deck slabs, offering a sustainable alternative to traditional construction methods.

Keywords: bubble deck concrete slabs, numerical homogenization, weight minimization, general nonlinear constitutive law, ultimate and serviceability limit states.

1. Introduction

The development of the construction industry has a significant and multifaceted impact on the natural environment. The construction process, the oper-

ation of buildings, and the subsequent management of waste generated during their use pose various ecological challenges. Therefore, modern construction engineering faces the imperative of developing methods and technologies aimed at minimizing environmental harm. Even at the design stage, the impact of buildings can be assessed from various perspectives, including raw material consumption, greenhouse gas emissions, environmental pollution and energy efficiency.

Traditional construction requires huge amounts of natural raw materials such as concrete, steel and wood, which significantly impact the environment [1]. The extraction and processing of these materials contribute to soil erosion, deforestation, and both water and air pollution. To reduce the consumption of natural resources, recycled materials can be used [2], or more efficient structures can be designed. However, this involves the use of advanced computational tools and the consideration of many factors, including structural stiffness and durability.

The use of materials with high-strength or special properties, combined with the optimization of the structural element shape allows for increased structural strength while simultaneously reducing material consumption. Examples include modern composites and materials that combine lightness with exceptional durability, as well as innovative technologies such as 3D printing. Interesting information about trends in composites used in construction can be found in [3, 4].

Another common technique in civil engineering for reducing structural weight while maintaining strength is the introduction of openings in structures. These perforations can be applied to a variety of structural elements. These include perforated steel beams, walls and partitions with openings, truss constructions, and floor slabs. This topic has been often discussed by scientists. For instance, Tsavdaridis and Mello [5] presented a comparison of perforated steel beams with different web opening shapes. Further insights on the design and impact of various cross-sectional parameters of perforated steel beams on their load-bearing capacity can be found in the papers of Akrami and Erfani [6] and Gajewski *et al.* [7]. Additionally, a nonlinear optimization approach for truss structures in buildings was presented by Smith *et al.* [8]. The mentioned papers focus only on analyses of perforated structures made of a single material type.

Challenges arise when dealing with hybrid structures, where different materials are combined in a single structural element. In such cases, it is necessary to take into account the specific mechanical properties of each material and their interactions, and this significantly complicates the analysis and design process. Hybrid structures, such as steel-concrete beams [9], carbon fiber composites [10], or floor slabs [11], combine the advantages of different materials, potentially offering better mechanical properties, including higher strength, enhanced durability and greater material efficiency. However, introducing perforations into these structures can lead to complex problems related to stress

concentration, different elastic-plastic properties and the behavior of materials under load. For this reason, in-depth strength analysis of such structural elements is so important.

Advanced analysis methods, such as the finite element method (FEM), play a crucial role here. FEM can be used to determine a wide range of problems, including the dynamic behavior of biaxial hollow slabs under human-induced loading [12], the assessment of thermal stresses in concrete airport runway slabs [13], and the analysis of the hole distribution in slabs subjected to harmonic loading [14]. Another example of using FEM in structures is presented in the paper by Al-Ansari *et al.* [15], which employed 3D FEM models to investigate the behavior of reinforced bubble deck concrete slabs exposed to fire. Also, Clement *et al.* [16] analyzed the punching resistance of concrete slabs using FEM. Unfortunately, modeling complex solid structures with perforations and additional reinforcements, such as truss elements, requires a refined mesh around the openings. This significantly increases the computational time and complexity of the analysis.

In-depth strength analysis also allows for design optimizations, which not only leads to material and cost savings during the construction stage but also reduces the carbon footprint of the project. Zhang *et al.* [17] proposed a pseudo-static topology optimization method for reinforced concrete walls. Furthermore, genetic algorithms were used for the optimal design of concrete structures in [18] and double parallel genetic algorithms [19]. Additionally, Yepes *et al.* [20] presented the application of a black hole algorithm for optimizing retaining walls. In [21], the authors presented a review of the literature on optimization approaches for reinforced concrete structures, particularly in the context of their impact on the natural environment. In addition, the following optimization algorithms can be distinguished in structural design: particle swarm [22], evolutionary [23], and metaheuristic [24].

This paper is a continuation of previous research on the analysis of floor slabs presented in [25, 26]. An algorithm is presented for determining the optimal cross-section of a structural element, exemplified by a concrete ceiling slab with steel reinforcement and uniformly distributed ellipsoidal holes. Unlike earlier studies, this work addresses both SLS) and ULS. For this purpose, an optimization is presented, which takes into account: (i) the structure's weight reduction, (ii) not exceeding the permissible deflection arrow under SLS, and (iii) maintaining stresses within allowable thresholds for both concrete and reinforcing steel under ULS. In this context, a GCL method is used, allowing for precise modeling of structure behavior by describing the relationships between stresses and strains. Additionally, a numerical homogenization technique based on strain energy equivalence between a simplified shell model and a 3D representative volume element (RVE) reference model of the slab, is applied. The

application of these methods significantly simplifies computational models and reduces the time required for strength analyses.

2. Materials and methods

2.1. Study framework and description of the optimization problem

The aim of this paper is to present a procedure for the optimal design of reinforced concrete bubble deck slabs, focusing on: (i) the minimal possible dead weight of concrete while simultaneously satisfying, (ii) ULS, and (iii) SLS. This is achieved by using fast computations through numerical homogenization of the slab, combined with the application of the general nonlinear constitutive law (GNCL) to a FEM analysis.

The design parameters considered in the optimization problem are: B – the size of the bubble deck unit, H – the height of the slab, and d_1 and d_2 – the horizontal and vertical diameters of the bubbles, respectively. A square base for the bubble deck unit is assumed. An exemplary bubble deck unit, along with the sought design parameters, is presented in Fig. 1. The lower and upper values of the design parameters are assumed according to reasonable physical limits, as outlined by Gajewski *et al.* [7], and are presented in Table 1.

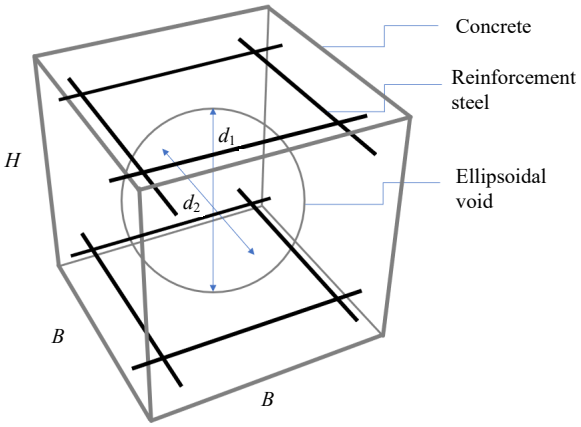

FIG. 1. Example of a bubble deck unit, showing the design parameters and the geometry of RVE.

TABLE 1. Limits of the design parameters for the bubble deck slab used in the optimization study.

Boundary	B [mm]	H [mm]	d_1 [mm]	d_2 [mm]
$b_{\min}$	100	100	50	50
$b_{\max}$	500	500	500	500

In Fig. 2, the overall view of the optimization procedure is presented. At the beginning, an initial guess for the design parameters $\mathbf{x}^0$ is assumed (denoted with a superscript 0), inspired by commercially available designs. Then, iteratively, the following procedure is repeated for different design parameters to find the global minimum of the cost function (CF) according to the optimization procedure.

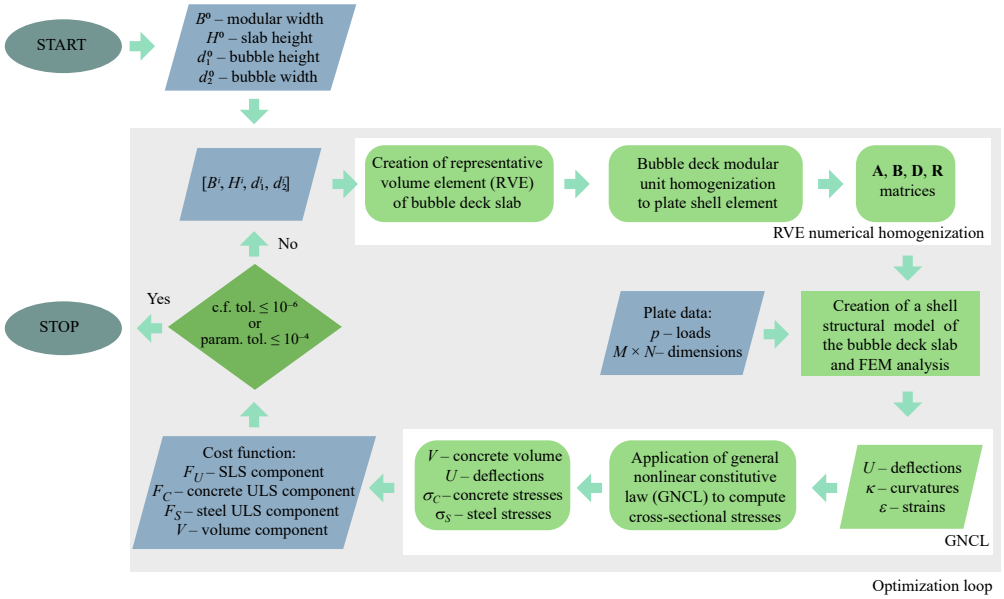

FIG. 2. Schematic illustration of the optimization loop with embedded methods, i.e., numerical bubble deck slab homogenization, FEM for modeling a free-supported slab, and the use of a GNCL to retrieve cross-sectional stresses.

For each evaluation of the CF F, first, the RVE of the bubble deck slab is built for the i-th design of the bubble deck, and then homogenized in order to obtain its properties, which are represented as a laminate. This involves calculating the **ABD** matrix [26]. An exemplary geometry of RVE is presented in Fig. 1. A brief explanation of the homogenization method used here is provided in Subsec. 2.2.

Then, the laminate properties are used as input for the constitutive law in the shell finite element method model of the bubble deck slab. The slab dimensions of the model are set to $8\ \mathrm{m} \times 12\ \mathrm{m}$. Additionally, it is assumed that the floor is situated within an office building and is subjected to uniformly distributed loads across the entire surface of the slab, as also considered in [26]. One of these loads is the live load with a characteristic value of $q_k = 3\ \mathrm{kN/m^2}$ (according to PN-EN 1990:2004; Eurocode 0: Basics of Structural Design, 2004). Moreover, it was assumed that the equivalent load from partition walls is $q_k = 0.8\ \mathrm{kN/m^2}$, and a permanent load, separate from the slab's own weight, has a value of

$g_k = 1.5$ kN/m^2. Additional details of the FEM model used, such as finite element type, mesh, and boundary conditions, are provided in Subsec. 2.3.

Because the structural FEM model of the slab can only compute the displacement field to satisfy SLS, the GNCL method was employed to calculate the cross-sectional stresses [27–30] to satisfy ULS. The GNCL method, fed with deflections U, curvatures κ, and strains ε, allows for the computation of stresses in the layers of the analyzed cross-section. Details of the GNCL method are presented in Subsec. 2.4.

The combined use of numerical homogenization for the bubble deck and the GNCL method enables the calculation of the deflection component of the optimization CF F_U (from the shell FEM model):

$$F_U(\mathbf{x}) = \left| U_{\max}(\mathbf{x}) - \frac{\min(M,N)}{250} \right|, \tag{1}$$

where $\mathbf{x}$ is the design parameter vector, $U_{\max}$ is the maximum deflection from the FEM analysis, and M and N are the dimensions of the slab.

Also, by employing a combination of these methods, it is possible to calculate the cross-sectional stress components of the CF. Specifically, F_C – the concrete stress component of the CF and F_S – the steel stresses component of the CF based on the maximum concrete stress σ_C, and maximum steel stress σ_S. In the GNCL method, the cross-sectional stresses are computed layer by layer along the cross-section's height. The expressions for F_C and F_S are as follows:

$$F_C(\overline{x}) = \left| R - \frac{\sigma_C(\mathbf{x})}{f_{cd}} \right|, \tag{2}$$

$$F_S(\overline{x}) = \left| R - \frac{\sigma_S(\mathbf{x})}{f_{yd}} \right|, \tag{3}$$

where R is the targeted load utilization rate, assumed to be 0.9 in this case. Moreover, f_{cd} is the design compressive strength of concrete; here, for C30/37 concrete, it equals 21.43 MPa, and f_{yd} is the design yield strength of steel; here, for B500SP steel, it equals 333.3 MPa.

The concrete volume component of the CF, V, is computed based on the assumed design parameters:

$$V_{\text{unit}}(\mathbf{x}) = B \cdot B \cdot H - \frac{4}{3}\pi \cdot \frac{d_1}{2} \cdot \frac{d_2}{2} \cdot \frac{d_2}{2}, \tag{4}$$

$$V(\mathbf{x}) = \frac{M \cdot N}{B^2} \cdot V_{\text{unit}}(\mathbf{x}), \tag{5}$$

where V_{unit} is the volume of concrete in a bubble deck unit.

Finally, the CF determined in the study takes the following form:

$$F(\overline{x}) = \omega_U F_U(\mathbf{x}) + \omega_C F_C(\mathbf{x}) + \omega_S F_S(\mathbf{x}) + \omega_{\text{vol}} V(\mathbf{x}), \tag{6}$$

where ω_i $(i = U, C, S, \text{vol})$ are dimensionless scaling factors, selected by trial and error to balance the influence of each component on the objective function. The values of ω_U, ω_C, ω_S, ω_{vol} were set to 1, 10, 10 and 0.1, respectively. All steps of the procedure (Fig. 2) were automated in MATLAB software to evaluate a single CF, including numerical homogenization, FEM computations, and GNCL calculations.

To minimize the assumed CF, the sequential quadratic programming method (SQP) was used. The details of the SQP method are described in Subsec. 2.5. In optimization, the following stopping criteria were applied:

$$\left|F\left(B^i,\, H^i,\, d_1^i,\, d_2^i\right) - F\left(B^{i+1},\, H^{i+1},\, d_1^{i+1},\, d_2^{i+1}\right)\right| \leq e_{fun}, \tag{7}$$

$$\left\|[B^i,\, H^i,\, d_1^i,\, d_2^i] - [B^{i+1},\, H^{i+1},\, d_1^{i+1},\, d_2^{i+1}]\right\| \leq e_{par}, \tag{8}$$

where e_{fun} and e_{par} are the tolerances for the convergence of CF and design parameters; here, set to 10^{-6} and 10^{-4}, respectively.

To improve the chances of finding the overall best solution (global minimum), given that the optimization method used is sensitive to local minimum values, multiple initial guesses for the design parameters were explored, see Table 2.

Table 2. Initial guesses of the design parameters selected for optimization of the concrete part of the bubble deck slab.

No.	B [mm]	H [mm]	d_1 [mm]	d_2 [mm]
$\mathbf{x}_1^0$	250	250	100	180
$\mathbf{x}_2^0$	300	280	130	130
$\mathbf{x}_3^0$	200	230	80	90
$\mathbf{x}_4^0$	280	240	160	140
$\mathbf{x}_5^0$	260	260	180	180

2.2. Numerical homogenization of the bubble deck slab

In the study, the numerical homogenization method was employed to construct a 3D solid representation of the bubble deck slab by using shell finite elements with realistic mechanical properties derived from the original design. In a similar manner, the numerical homogenization method was used in previous studies on bubble deck design, such as those focusing on sensitivity analysis [25] and the optimization concerning SLS only [26]. Given that the homogenization method used here closely follows these earlier works, it will only be briefly reviewed in this subsection, and for more details, see the previous papers.

The numerical homogenization method used in this study is based on the balance of strain energy between the 3D bubble deck unit model and its simplified shell model [31,32]. This method has been applied not only to bubble deck slabs but also to concrete slabs reinforced with spatial trusses [33]. In this approach, the classical FEM equation is decomposed internal and external nodes of the FE mesh:

$$\mathbf{K}\,\mathbf{u} = \mathbf{F} \;\rightarrow\; \begin{bmatrix} \mathbf{K}_{ee} & \mathbf{K}_{ei} \\ \mathbf{K}_{ie} & \mathbf{K}_{ii} \end{bmatrix} \begin{bmatrix} \mathbf{u}_e \\ \mathbf{u}_i \end{bmatrix} = \begin{bmatrix} \mathbf{F}_e \\ \mathbf{0} \end{bmatrix}. \tag{9}$$

In this equation, i refers to the internal nodes, while e refers to the external nodes. In classical FE terms, $\mathbf{K}$ is the global stiffness matrix, $\mathbf{u}$ is the displacement vector representing the degrees of freedom of the nodes, and $\mathbf{F}$ is the external nodal load vector. The internal nodes of the 3D model of the bubble deck slab unit are excluded by applying the static condensation. Therefore, the elastic strain energy is defined as follows:

$$E = \frac{1}{2}\mathbf{u}_e^{\mathrm{T}}\,\mathbf{K}\,\mathbf{u}_e = \frac{1}{2}\boldsymbol{\epsilon}_e^{\mathrm{T}}\,\mathbf{A}_e^{\mathrm{T}}\,\mathbf{K}\,\mathbf{A}_e\,\boldsymbol{\epsilon}_e. \tag{10}$$

For a single node, we obtain:

$$\mathbf{u}_e = \mathbf{A}_e\boldsymbol{\epsilon}_e. \tag{11}$$

In full form:

$$\begin{bmatrix} u_x \\ u_y \\ u_z \end{bmatrix} = \begin{bmatrix} x & 0 & y/2 & z/2 & 0 & xz & 0 & yz/2 \\ 0 & y & x/2 & 0 & z/2 & 0 & yz & xz/2 \\ 0 & 0 & 0 & x/2 & y/2 & -x^2/2 & -y^2/2 & -xy/2 \end{bmatrix} \begin{bmatrix} \varepsilon_x \\ \varepsilon_y \\ \gamma_{xy} \\ \gamma_{xz} \\ \gamma_{yz} \\ \kappa_x \\ \kappa_y \\ \kappa_{xy} \end{bmatrix}, \tag{12}$$

where u_x, u_y, and u_z are node displacements in three directions, ε_x and ε_y are membrane strains, γ_{xy}, γ_{xz}, and γ_{yz} are transverse shear strains, and κ_x, κ_y, and κ_{xy} are curvatures. Equation (12) describes how each of the strain components contributes to the displacements at a given node, depending on its spatial coordinates x, y, and z.

The internal elastic energy for the shell can further be expressed as:

$$E = \frac{1}{2}\boldsymbol{\epsilon}_e^{\mathrm{T}}\,\mathbf{A}_{\mathrm{k}}\,\boldsymbol{\epsilon}_e\{\mathrm{area}\}. \tag{13}$$

The homogenization method thus allows for the extraction of the stiffness matrix in a discrete form as:

$$\mathbf{A}_k = \frac{\mathbf{A}_e^{\mathrm{T}}\,\mathbf{K}\,\mathbf{A}_e}{\text{area}}, \tag{14}$$

where $\mathbf{A}_k$ is the extended laminate stiffness matrix, which is composed of $\mathbf{A}$, $\mathbf{B}$, $\mathbf{D}$, and $\mathbf{R}$ submatrices, which are tension/compression stiffnesses matrix, coupling matrix, bending stiffness matrix and transverse shear stiffness matrix, respectively.

2.3. Numerical models used in the study

In the paper, three different numerical models were used: (a) a full 3D model for the proposed method validation, (b) a shell model for optimization analyses, and (c) an RVE model for accurate determination of the stiffness matrix.

In order to validate the proposed bubble deck optimization method, reference values for deflections and stresses were calculated for the full 3D model of the plate. For this purpose, the commercial FE software (ABAQUS FEA) [34] was used. The results obtained from the 3D model were then compared with the results obtained from the simplified shell model, which employed numerical homogenization (described in Subsec. 2.2) and the GNCL method (described in Subsec. 2.4). The bubble deck plate was designed as a plate simply supported along all four edges and subjected to an evenly distributed load across the entire surface, as presented in Subsec. 2.1.

In the reference model, the slab was modeled as a 3D solid concrete structure with the following dimensions: 12.0 m length, 8.0 m width and 0.30 m thickness. The reinforcement was modeled as steel wire structures in two directions, placed on both the upper and lower surfaces. The reinforcement mesh, consisting of bars with a diameter of $\varphi = 12$ mm and an average spacing of 150 mm, was anchored in the concrete slab using the embedded techniques available in the ABAQUS FEA software [34].

The concrete part of the model was divided into 10-node brick elements, each with three degrees of freedom per node (C3D10R solid elements according to [34]), with a representative dimension of 0.05 m. The steel elements were modeled using 2-node truss elements with three degrees of freedom per node (T3D2 truss elements according to [34]). The total number of nodes in the solid elements was equal to 1 376 048, while the truss elements had 24 896 nodes, resulting in a total of over 6.4 million degrees of freedom.

Two constitutive models were used to describe the mechanical properties of the bubble deck: concrete was modeled by a linear stress-strain relationship and steel was represented by an elastic perfectly-plastic law. Table 3 presents the

TABLE 3. Material properties of steel and concrete used in the analyses.

Material	E [GPa]	ν [–]	f_{yk} [MPa]	f_{ck} [MPa]	f_{cm} [MPa]	f_{ctk} [MPa]
Steel	210	0.3	500	–	–	–
Concrete	32	0.2	–	30	38	2.0

engineering parameters of the materials, where E is Young's modulus, ν is Poisson's ratio, f_{yk} is the characteristic value of yield strength of steel. The remaining parameters concern the characteristics of concrete: f_{ck} is the characteristic cylindrical compressive strength, f_{cm} is the average value of the compressive strength and f_{ctk} is the characteristic value of tension strength.

The second, simplified model of the plate was created as a shell model with the same width and length as the 3D model. Additionally, the support conditions and the applied load were consistent with the bubble deck reference model. The mechanical properties were described using equivalent stiffnesses obtained by numerical homogenization of the RVE (see Subsec. 2.2). The shell model was divided into 4-node, quadrilateral, stress/displacement shell elements (S4R) with representative dimensions of 0.50 m. The total number of elements was equal to 384, which is approximately 3850 times smaller than in the reference model.

Moreover, in numerical homogenization analyses, in order to properly define the stiffness matrix of the model, it is necessary to appropriately extract the RVE of the bubble deck. The RVE was obtained by isolating a periodic fragment of the structure from the entire 3D model. The external dimensions of the RVE and the bubble (vertical and horizontal diameters) were the variables depending on the optimization task. The design parameters of the bubble deck slab were presented in Fig. 1. The slab reinforcement was modeled as truss elements with a diameter of $\varphi = 12$ mm, spaced every 125 mm. The bars inside the slab were arranged in two directions at two levels: top and bottom. The properties of the materials used (i.e., steel and concrete) were presented in Table 3. The reinforcement was modeled by using 2-node truss-type elements (T3D2), and the concrete slab was meshed with 10-node brick elements (C3D10) with a representative dimension of 0.05 m. It must be underlined that the RVE model was used only for computing the stiffness matrix for the numerical homogenization purpose. No formal FEM computations are required for obtaining the laminate properties for modeling the slab while using numerical homogenization, as described in [32].

2.4. Application of general nonlinear constitutive law

The GNCL method was used in this work for calculating the cross-sectional stresses after numerical homogenization. The GNCL method enables the con-

sideration of nonlinear mechanical properties of the material, such as plasticity, viscosity and damage processes, which are crucial for accurately modeling and predicting the behavior of real materials under complex stress states.

The foundations of GNCL method were established several decades ago. In 1982, Łodygowski first applied it to the analysis of beams and plane frames, incorporating geometric nonlinearities [35]. Then, the method was extended in a two-stage bending analysis of composite beams by dividing the section into layers [36]. Later, in [27], the above method was extended to include Timoshenko's theory. In addition, the GNCL method was used for nonlinear analysis of composite beams [28], trapezoidal sheets [29], and prestressed channel slabs [30].

The analysis presented here was carried out in accordance with the scheme presented in Fig. 2. In the optimization loop, the numerical homogenization method and the FEM were used to obtain element displacements, which in the next step were used in the GNCL method to calculate the stresses in the slab. For this purpose, it is necessary to determine the deformations (normal strains ε_0 in both directions and corresponding curvatures $\kappa(x)$ and $\kappa(y)$) occurring in the cross-section under consideration. In this study, since the largest deformations occur at the midspan, only in this cross-section the GNCL method calculations were performed only at this specific cross-section, based on the nodal displacements.

In x-direction of the plate, normal strains can be determined according to the following formula, which represents the ratio of element elongation ΔL to the length L:

$$\varepsilon_0 = \frac{\Delta L}{L} = \frac{u_2 - u_1}{L}, \tag{15}$$

where u_1, u_2 are the nodal displacements at the two nodes along the element.

It was assumed that the shape function has the form of a 3rd degree polynomial

$$v(x) = C_3 x^3 + C_2 x^2 + C_1 x + C_0. \tag{16}$$

Based on the boundary conditions, the polynomial constants are determined using the following equations:

$$\begin{aligned} &x = 0, \qquad v(0) = v_1, \qquad \frac{\mathrm{d}v(0)}{\mathrm{d}x} = \varphi_1, \\ &x = L, \qquad v(L) = v_2, \qquad \frac{\mathrm{d}v(L)}{\mathrm{d}x} = \varphi_2. \end{aligned} \tag{17}$$

For small displacement framework, the curvature formula can be simplified and only the second derivative of the transverse deflection can be used:

$$\kappa(x) = \frac{\mathrm{d}^2 v}{\mathrm{d}x^2}. \tag{18}$$

After this simplification, the curvature can be calculated according to the following formula:

$$\kappa(x) = -\frac{2}{L^3}\left[\varphi_1 L(2L-3x) + \varphi_2 L(L-3x) + 3(v_1-v_2)(L-2x)\right]. \tag{19}$$

In this approach, the representative curvature $\overline{\kappa}$ is defined as the weighted average of the curvatures calculated at the three points using Gaussian quadrature:

$$\overline{\kappa} = B_1\kappa_1 + B_2\kappa_2 + B_3\kappa_3, \tag{20}$$

where B_1, B_2, B_3 are the weights for the Gaussian quadrature points $B_1 = 5/18$, $B_2 = 4/9$, and $B_3 = 5/18$, and κ_1, κ_2, κ_3 are curvatures calculated at three Gaussian points $x_1 = 1/9\,L$, $x_2 = 1/2\,L$, and $x_3 = 8/9\,L$.

The above calculations of $\kappa(x)$ are presented for the x-direction of the plate. For the other plate direction, i.e., y, the calculations were performed according to the same algorithm, but with the appropriate dimensions.

The combination of the GNCL with the homogenization method enables the calculation of stresses in the bubble deck slab cross-section using shell model with heterogeneous material. A layered approach was used for this purpose, where the slab cross-section was divided into thin layers, each 1 millimeter thick. During the deformation analysis (FE shell model), the entire cross-section, consisting of both concrete and steel parts, is assumed to be homogeneous, but with representative parameters derived from numerical homogenization. When analyzing stresses using GNCL, the concrete and steel parts are taken into account separately.

Curvatures determined by Eqs. (18)–(20) were calculated separately for the two directions of the plate. Then, based on these, the stresses occurring at the middle of the span of the analyzed structural element were determined separately for steel and concrete. The stresses were determined according to Eq. (21):

$$\sigma = E\varepsilon_0 + E\kappa(y_g - y_i), \tag{21}$$

where E is Young's modulus separately for steel and concrete, ε_0 is the normal strain, κ is the curvature, y_g and y_i are the positions of the neutral axis of the whole section and the i-th layer relative to its top edge, respectively.

2.5. Mathematical optimization procedure

In this subsection, we provide a brief description of the optimization method employed in this study – sequential quadratic programming (SQP). SQP is recognized as one of the most reliable and effective minimization algorithms for

this type of problem. Benchmark examples have demonstrated their ability to achieve sufficient accuracy with a limited number of CF evaluations [37–41]. Additionally, its success has been reported in various optimization studies, such as [26], and in similar optimization problems, as exemplified by [25].

From a mathematical point of view, solving the optimization problem involves minimizing the CF assumed $F(\mathbf{x})$ for design parameters $\mathbf{x}$, subject to its linear constraints:

$$\begin{aligned} &C_{eq}(\mathbf{x}) = 0, \\ &A_{eq} \cdot \mathbf{x} = b_{eq}, \end{aligned} \tag{22}$$

or/and nonlinear constraints:

$$\begin{aligned} &C(\mathbf{x}) \leq 0, \\ &A \cdot \mathbf{x} \leq b, \\ &b_{\min} \leq \mathbf{x} \leq b_{\max}, \end{aligned} \tag{23}$$

where b and b_{eq} are column vectors, A and A_{eq} are matrices, C and C_{eq} are functions, and $b_{\min}$ and $b_{\max}$ are the limits of the design parameters $\mathbf{x}$.

Lagrange's function is used to incorporate the nonlinear constraints of the CF $F(\mathbf{x})$:

$$L(\overline{x}, \lambda) = F(\mathbf{x}) + \sum_{i=1}^{m} \lambda_i \cdot g(\mathbf{x}), \tag{24}$$

where λ_i are the Lagrange multipliers, while $g_i(\mathbf{x})$ are the nonlinear constraints.

In fact, in the SQP method, the substitute quadratic problem, which approximates above equation, is solved iteratively:

$$\min_{d \in E^n} \frac{1}{2} d^{\mathrm{T}} H_k d + \nabla F(\mathbf{x}_k)^{\mathrm{T}} d, \tag{25}$$

where H_k is the positive-definite approximation of the Hessian matrix. For the Hessian matrix approximation, the Broyden–Fletcher–Goldfarb–Shanno (BFGS) method was utilized in the paper. For more details of the method, see the original papers [42–45].

3. Results

3.1. Computational verification of the proposed method

In order to validate the proposed method of analyzing structures at the ultimate and serviceability limit states using numerical homogenization and

the GNCL method, additional numerical analyses of the full 3D bubble deck model were performed. The obtained results for stresses and displacements from the reference model were compared with the results obtained from the simplified shell model. The maximum displacement of the slab, stresses at the extreme fibers of the concrete part, and the reinforcement in two directions are shown in Table 4. The values shown were taken from the center of the slab, where the displacements and stresses are largest.

Table 4. Comparison between the physical values computed by the full solid finite element model and those derived by numerical homogenization and the application of GNCL using the shell finite element model.

Physical quantity	Full solid model	Homogenized shell model with GNCL	Homogenization error [%]
u_y [mm]	4.261	4.389	3.00
$\sigma_x^{\text{concrete}}$ [MPa]	3.380	3.225	4.59
$\sigma_z^{\text{concrete}}$ [MPa]	1.899	1.796	5.42
σ_x^{steel} [MPa]	8.638	8.315	3.74

The discrepancy in displacements between the proposed method and the 3D model is 3.0%. However, the stress difference between models ranges from 3.7% to 5.4%. The obtained results differ slightly, which confirms the validity of the proposed method.

3.2. Optimization analyses

Table 5 summarizes the results of five optimization analyses that yielded the lowest final objective function values. Several cases with significantly higher final objective function values were omitted. In addition to the final input parameter values (columns 2–5), i.e., B, H, d_1, and d_2, Table 5 also includes information on the plate's maximal deflection w, the concrete volume of the entire slab V (calculated according to Eq. (5)), maximum stresses in concrete σ_C,

Table 5. Optimal designs of the concrete bubble deck slab with corresponding CF values obtained by the optimization algorithm.

	B [mm]	H [mm]	d_1 [mm]	d_2 [mm]	w [mm]	V [m^3]	σ_C [MPa]	σ_S [MPa]	$F(\mathbf{x}_i^{opt})$ [–]
$\mathbf{x}_1^{opt}$	465.0	141.5	67.4	395.0	32.0	11.14	13.44	41.33	11.637
$\mathbf{x}_2^{opt}$	500.0	141.6	71.6	114.3	32.0	13.41	9.68	41.39	13.879
$\mathbf{x}_3^{opt}$	500.0	142.4	72.4	429.1	31.8	11.00	14.66	41.56	11.161
$\mathbf{x}_4^{opt}$	134.0	138.3	68.3	62.1	32.0	12.54	9.43	39.39	13.692
$\mathbf{x}_5^{opt}$	500.0	142.1	64.1	102.5	32.0	13.51	9.63	41.21	13.645

and in reinforcement σ_S (columns 6–9). Additionally, the last column presents the obtained objective function value for each analysis, which was computed according to Eq. (6).

In the following section of the article, selected results from individual optimization analyses are presented. As examples, the cases chosen correspond to the lowest values of the objective function obtained during the optimization process. Specifically, examples presented were based on the initial parameters $\mathbf{x}_1^0$ and $\mathbf{x}_3^0$, as shown in Table 2. For these cases, the final values of the objective function were 11.637 and 11.161 for $\mathbf{x}_1^{opt}$ and $\mathbf{x}_3^{opt}$, respectively, as detailed in Table 5.

The detailed results of the optimization analyses are presented in the convergence graphs of the optimization process, showing how the solution approaches the optimal values with the smallest objective function. Figures 3a and 4a illustrate this convergence for the initial parameters $\mathbf{x}_1^0$ and $\mathbf{x}_3^0$, respectively. These plots show the components of the objective function according to Eq. (6). More-

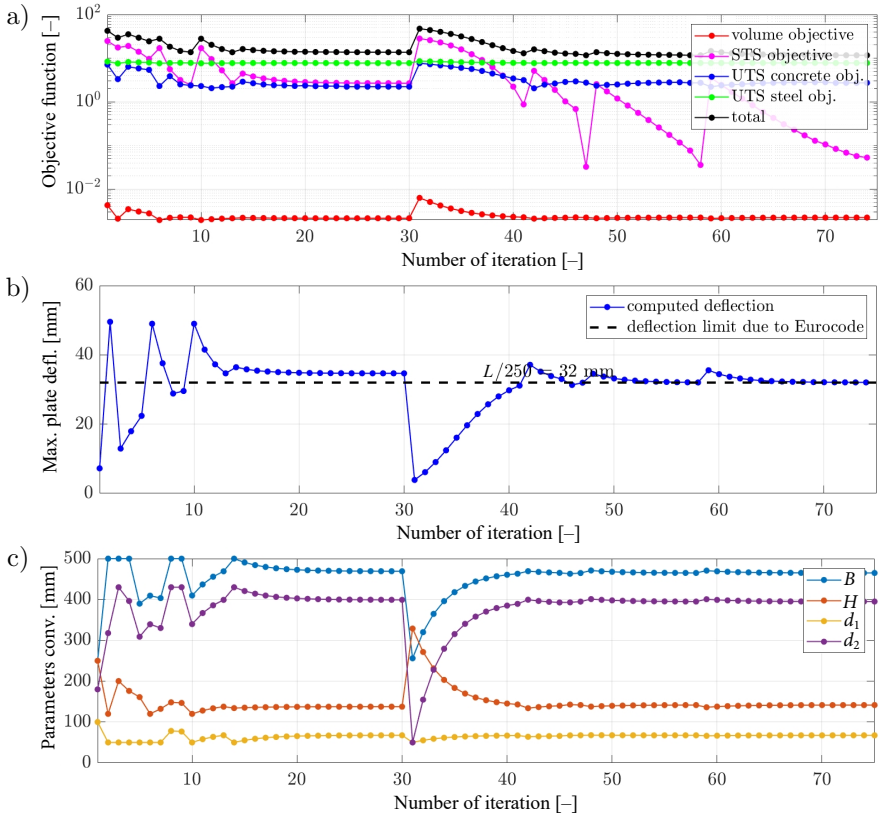

FIG. 3. The convergence of the optimization of geometrical parameters of slab for initial parameters $\mathbf{x}_1^0$: a) objective function, b) the serviceability limit state, and c) corresponding bubble deck parameters.

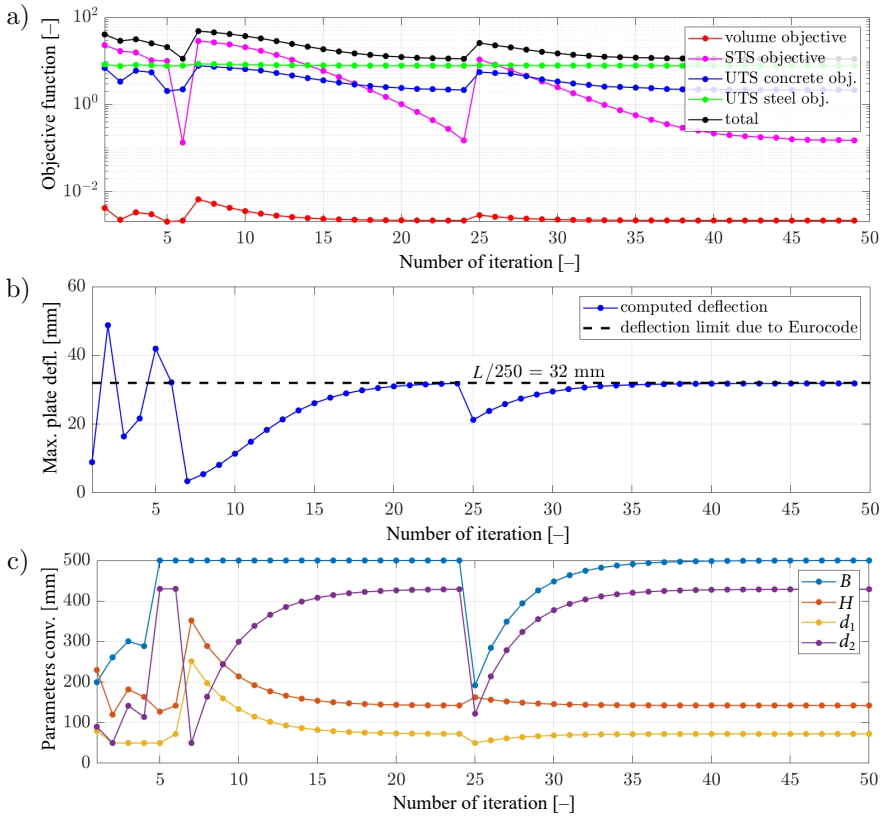

FIG. 4. The convergence of the optimization of geometrical parameters of slab for initial parameters $\mathbf{x}_3^0$: a) objective function, b) the serviceability limit state, and c) corresponding bubble deck parameters.

over, Figs. 3b and 4b show the resulting values of the calculated maximum displacement of the slab based on the FEM analysis, compared to the ULS limit for the slab considered (indicated by the dashed line). In addition, Figs. 3c and 4c demonstrate the changes in design parameter values during the iterative optimization process, starting from the initial parameters $\mathbf{x}_1^0$ and $\mathbf{x}_3^0$, respectively.

4. Discussion

The summary of the results achieved in the study is presented in Table 5. It can be observed that the CF values obtained range between approx. 11.16 and 13.69. The CF for the $\mathbf{x}_1^{opt}$ and $\mathbf{x}_3^{opt}$ cases are much lower than for the other cases. Among these, the best solution was obtained for $\mathbf{x}_3^{opt}$ with the optimal design parameters vector equal to [500.0, 142.4, 72.4, 429.1], as shown in Table 5.

The optimal parameters and their corresponding CF values, as presented in Table 5, vary, indicating the presence of local minima. Specifically, the parameter B predominantly takes values at the upper boundary, around 500 mm, while H fluctuates closely around 141 mm. In a similar manner, d_1 tends to remain close to 70 mm. In contrast, d_2 exhibits a wider range varying from about 62 mm to even 429.1 mm, indicating a less conservative approach.

The CF, as defined in this study, depends on w, V, σ_C, and σ_S. The deflections obtained for the cases shown in Table 5 are close to 32 mm, which corresponds to the deflection limit or this structure according to SLS (8000 mm/250 = 32 mm). Here, in almost all cases shown, the result obtained reaches the limit value, which confirms that this is an important component in CF. The volume of the concrete V is correlated with the CF outcome, as shown in columns 7 and 10.

When analyzing the ULS limit, the stresses in concrete σ_C and steel σ_S are computed by the GNCL approach. The stresses obtained in the optimal solutions are well below the design compressive strength of concrete and the yield strength of steel, i.e., 21.43 MPa and 333.3 MPa, respectively. In fact, the compression stress in the concrete does not exceed 14.7 MPa, meaning the utilization of the concrete's load capacity is less than 68% in the worst case. For steel, the maximum stress is less than 42.0 MPa, resulting in a load capacity utilization of less than 13% in the worst case.

The following results present selected optimization examples, focusing on the best solutions, with particular attention to the first and third cases. In the first case, we observe a gradual decrease in the objective function values with occasional, local increases. Throughout the optimization process, each component of the objective function ultimately decreases, as shown in Fig. 3a. The influence of the deflection (SLS objective) and the concrete load capacity (ULS concrete objective) is significant, while the volume of concrete has a much smaller impact, and the influence of steel stress (ULS steel objective) is minimal. For instance, in iterations 2-3, 9-10, and 30-31, there is a noticeable increase in the objective function values and its components, particularly with respect to the SLS and ULS concrete objectives, as well as the concrete volume. However, in iterations 41-42 and 58-59, the sudden change in deflection is less pronounced in the other components, resulting in no significant change in the overall objective function.

The same trend can be observed in Fig. 3b, where the slab deflection approaches the limit value of 32 mm, eventually reaching it by the end of the optimization process. In Fig. 3c, the initial fluctuation in the objective function corresponds to changes in all design parameters. By the 14th iteration, these trends begin to stabilize. In the 30th iteration, there is a sudden change in the height and width of the RVE, as well as the horizontal diameter of the bubble. However, these trends stabilize once again in subsequent iterations. From this

point onward, the optimization algorithm makes only slight adjustments to the parameter values with each iteration.

In the next example, which represents the third case, we also observe initial fluctuations in the components of the objective function and design parameters, as shown in Figs. 4a and 4c. However, stabilization occurs more quickly in this case. Here, similar to the first case, the deflection (SLS objective) and concrete load capacity (ULS concrete objective) have the biggest impact, while the volume of the concrete has a much smaller effect, and the influence of steel stress (ULS steel objective) is small. Notable increases in the objective function values and its components, particularly in the SLS, ULS concrete, and volume, are seen in iterations 6-7 and 24-25. The tendency to achieve the maximum displacement values is also evident, as depicted in Fig. 4b, where the most dynamic changes occur in iterations 6-7 and 24-25, followed by gradual convergence to the optimal values.

As demonstrated in this study, it is possible to achieve optimal selection of design parameters to minimize a complex objective function that considers various aspects of the bubble deck slab structure. One important consideration and limitation of this study is the chosen set of weight parameters for the components of the objective function. Here, these parameters were selected based on preliminary studies and are considered by the authors to be useful factors for solving practical design tasks. For the chosen set of weight factors, it was found that one of the most crucial criteria identified was the deflection of the structure, which significantly influenced the optimization algorithm's decisions.

The presented research results cannot be compared to existing literature because, to the best of our knowledge, studies of this slab type represent a unique contribution to the scientific literature. Experimental validation of the results presented here is planned as a part of forthcoming research.

5. Conclusions

This study presented an effective procedure for the optimal design of reinforced concrete bubble deck slabs, focusing on minimizing dead weight while ensuring compliance with ULS and SLS requirements. The main novelty of this work is the methodology, which integrates numerical homogenization and a GNCL within an FEM framework for quick and precise computations. By avoiding the need to build complex and expensive finite element models, the approach achieved high precision while significantly reducing computational costs.

This approach enabled to identify slab configurations that minimize the CF while meeting structural demands. Numerical homogenization and GNCL methods provided accurate evaluation of slab behavior. Numerical homogenization

yielded reliable laminate properties, while the GNCL method calculated cross-sectional stresses, ensuring a comprehensive evaluation of slab performance. The CF considered in the study included deflections, concrete volume, concrete stresses and steel stresses, resulting in a balanced structure that optimizes load capacity and material cost. Automating the entire procedure and employing the sequential quadratic programming method enabled efficient optimization and reliable results.

In summary, the proposed optimization procedure offers a robust and flexible tool for designing efficient and sustainable reinforced concrete bubble deck slabs.

Acknowledgements

The authors would like to acknowledge the grant from the Ministry of Education and Science, Poland, for Young Researchers at Poznan University of Technology; grant number 0411/SBAD/0009.

Author contributions

Conceptualization Tomasz Garbowski (T.Gar.); methodology Natalia Staszak (N.S.), Tomasz Gajewski (T.Gaj.) and T.Gar.; software N.S. and T.Gaj.; validation T.Gaj. and N.S.; formal analysis T.Gaj. and N.S.; investigation N.S. and T.Gaj.; writing – original draft preparation T.Gaj. and N.S.; writing – review and editing T.Gaj., T.Gar., and N.S.; visualization T.Gaj. and N.S.; supervision T.Gar. and T.Gaj.; funding acquisition T.Gar. All authors have read and agreed to the published version of the manuscript.

Data availability statement

The data presented in this study are available upon request from the corresponding author.

Conflicts of interest

The authors declare no conflict of interest. The funders had no role in the design of the study, in the collection, analyses, or interpretation of data, in the writing of the manuscript, or in the decision to publish the results.

References

1. S.G. Maxineasa, N. Taranu, Traditional building materials and fibre reinforced polymer composites. A sustainability approach in construction sector, *Journal Bulletin of the Polytechnic Institute of Iaşi. Construction. Architecture Section*, **59**(2): 55–68, 2013.

2. G. Petkovic, C.J. Engelsen, A.O. Håøya, G. Breedveld, Environmental impact from the use of recycled materials in road construction: Method for decision-making in Norway, *Resources, Conservation and Recycling*, **42**(3): 249–264, 2004, https://doi.org/10.1016/j.resconrec.2004.04.004.

3. E.P. Dorofeev, N.N. Dorofeeva, Composites as a modern trend, *IOP Conference Series: Materials Science and Engineering*, **1079**(4): 042052, 2021, https://doi.org/10.1088/1757-899X/1079/4/042052.

4. P.G. Kossakowski, W. Wciślik, Fiber-reinforced polymer composites in the construction of bridges: Opportunities, problems and challenges, *Fibers*, **10**(4): 37, 2022, https://doi.org/10.3390/fib10040037.

5. K.D. Tsavdaridis, C. D'Mello, Finite element investigation of perforated steel beams with different web opening configurations, [in:] *Proceedings of the 6th International Conference on Advances is Steel Structures (ICASS 2009)*, Hong Kong, China, 16–18 December 2009, pp. 213–220.

6. V. Akrami, S. Erfani, Review and assessment of design methodologies for perforated steel beams, *Journal of Structural Engineering*, **142**(2): 04015148, 2016, https://doi.org/10.1061/(ASCE)ST.1943-541X.0001421.

7. T. Gajewski, N. Staszak, T. Garbowski, Parametric optimization of thin-walled 3D beams with perforation based on homogenization and soft computing, *Materials*, **15**(7): 2520, 2022, https://doi.org/10.3390/ma15072520.

8. J. Smith, J. Hodgins, I. Oppenheim, A. Witkin, Creating models of truss structures with optimization, *ACM Transactions on Graphics*, **21**(3): 295–301, 2002, https://doi.org/10.1145/566654.566580.

9. P. Colajanni, L.L. Mendola, A. Monaco, Review of push-out and shear response of hybrid steel-trussed concrete beams, *Buildings*, **8**(10): 134, 2018, https://doi.org/10.3390/buildings8100134.

10. T. George, V.S. Deshpande, H.N.G. Wadley, Hybrid carbon fiber composite lattice truss structures, *Composites Part A: Applied Science and Manufacturing*, **65**: 135–147, 2014, https://doi.org/10.1016/j.compositesa.2014.06.011.

11. M. Hosseini *et al.*, Numerical study on the behaviour of hybrid FRPs reinforced RC slabs subjected to blast loads, *Journal of Renewable Materials*, **11**(9): 3517–3531, 2023, https://doi.org/10.32604/jrm.2023.028164.

12. T. Mota, M.H. Oliveira, G. Doz, Dynamic analysis in a bi-axial hollow slab submitted to human actions, *Revista IBRACON de Estruturas e Materiais*, **17**(6): e17608, 2024, https://doi.org/10.1590/S1983-41952024000600008.

13. T. Shimomura, T. Nishizawa, T. Ozeki, Evaluation of thermal stress in airport concrete pavement slab by 3D-FEM analysis, [in:] *9th International Conference on Concrete Pavements, International Society for Concrete Pavements*, San Francisco, California, United States, 17–21 August 2008, pp. 740–754, 2008.

14. A.S. Mahdi, S.D. Mohammed, Experimental and numerical analysis of bubbles distribution influence in BubbleDeck Slab under harmonic load effect, *Engineering, Technology & Applied Science Research*, **11**(1): 6645–6649, 2021, https://doi.org/10.48084/etasr.3963.

15. A.A. Al-Ansari, M.M. Kharnoob, M.A. Kadhim, Abaqus Simulation of the Fire's Impact on Reinforced Concrete Bubble Deck Slabs, [in:] *E3S Web of Conferences. International*

Conference on Geotechnical Engineering and Energetic-Iraq (ICGEE 2023), Vol. 427, Article no. 02001, 2023, https://doi.org/10.1051/e3sconf/202342702001.

16. T. Clement, A.P. Ramos, M.F. Ruiz, A. Muttoni, Design for punching of prestressed concrete slabs, *Structural Concrete*, **14**(2): 157–167, 2013, https://doi.org/10.1002/suco.201200028.

17. H.Z. Zhang, Z.S. Wu, H. Chen, Z.L. Ma, P. Luo, Pseudo-static topology optimization using the evolutionary-type method for reinforced concrete shear walls, *Engineering Optimization*, **57**(6): 1445–1466, 2025, https://doi.org/10.1080/0305215X.2024.2355332.

18. E.M. Fairbairn, M.M. Silvoso, R.D. Toledo Filho, J.L. Alves, N.F. Ebecken, Optimization of mass concrete construction using genetic algorithms, *Computers & Structures*, **82**(2-3): 281–299, 2004, https://doi.org/10.1016/j.compstruc.2003.08.008.

19. M. Rita, E. Fairbairn, F. Ribeiro, H. Andrade, H. Barbosa, Optimization of mass concrete construction using a twofold parallel genetic algorithm, *Applied Sciences*, **8**(3): 399, 2018, https://doi.org/10.3390/app8030399.

20. V. Yepes, J.V. Martí, J. García, Black hole algorithm for sustainable design of counterfort retaining walls, *Sustainability*, **12**(7): 2767, 2020, https://doi.org/10.3390/su12072767.

21. M. Afzal, Y. Liu, J.C. Cheng, V.J. Gan, Reinforced concrete structural design optimization: A critical review, *Journal of Cleaner Production*, **260**: 120623, 2020, https://doi.org/10.1016/j.jclepro.2020.120623.

22. M.A. Jayaram, M.C. Nataraja, C.N. Ravikumar, Design of high performance concrete mixes through particle swarm optimization, *Journal of Intelligent Systems*, **19**(3): 249–264, 2010, https://doi.org/10.1515/JISYS.2010.19.3.249.

23. M. Schnellenbach-Held, J.E. Habersaat, Bionic optimization of concrete structures by evolutionary algorithms, *Structural Engineering International*, **24**(2): 229–235, 2014, https://doi.org/10.2749/101686614X13830790993564.

24. A. Kaveh, K.B. Hamedani, S.M. Hosseini, T. Bakhshpoori, Optimal design of planar steel frame structures utilizing meta-heuristic optimization algorithms, *Structures*, **25**: 335–346, 2020, https://doi.org/10.1016/j.istruc.2020.03.032.

25. N. Staszak, T. Garbowski, B. Ksit, Optimal design of bubble deck concrete slabs: Sensitivity analysis and numerical homogenization, *Materials*, **16**(6): 2320, 2023, https://doi.org/10.3390/ma16062320.

26. T. Gajewski, N. Staszak, T. Garbowski, Optimal design of bubble deck concrete slabs: Serviceability limit state, *Materials*, **16**(14): 4897, 2023, https://doi.org/10.3390/ma16144897.

27. D. Mrówczyński, T. Gajewski, T. Garbowski, Application of the generalized nonlinear constitutive law in 2D shear flexible beam structures, *Archives of Civil Engineering*, **67**(3): 157–176, 2021, https://doi.org/10.24425/ace.2021.138049.

28. D. Mrówczyński, T. Gajewski, T. Garbowski, The generalized constitutive law in nonlinear structural analysis of steel frames, [in:] *Modern Trends in Research on Steel, Aluminium and Composite Structures, Proceedings of the 14th International Conference on Metal Structures, Poznań, Poland, 16–18 June 2021*, M.A. Giżejowski, A. Kozłowski, M. Chybiński, K. Rzeszut, R. Studziński, M. Szumigała [Eds.], pp. 120–126, Routledge, London, 2021, https://doi.org/10.1201/9781003132134-12.

29. N. Staszak, T. Gajewski, T. Garbowski, Generalized nonlinear constitutive law applied to steel trapezoidal sheet plates, [in:] *Modern Trends in Research on Steel, Aluminium and Composite Structures, Proceedings of the 14th International Conference on Metal Structures (ICMS2021): Poznan, Poland, 16–18 June 2021*, M.A. Gizejowski, A. Kozłowski, M. Chybiński, K. Rzeszut, R. Studziński, M. Szumigała [Eds.], pp. 185–191, Routledge, London, 2021, https://doi.org/10.1201/9781003132134-21.

30. N. Staszak, T. Garbowski, B. Ksit, Application of the generalized nonlinear constitutive law in numerical analysis of hollow-core slabs, *Archives of Civil Engineering*, **68**(2): 125–145, 2022, https://doi.org/10.24425/ace.2022.140633.

31. M.E. Biancolini, Evaluation of equivalent stiffness properties of corrugated board, *Composite Structures*, **69**(3): 322–328, 2005, https://doi.org/10.1016/j.compstruct.2004.07.014.

32. T. Garbowski, T. Gajewski, Determination of transverse shear stiffness of sandwich panels with a corrugated core by numerical homogenization, *Materials*, **14**(8): 1976, 2021, https://doi.org/10.3390/ma14081976.

33. N. Staszak, T. Garbowski, A. Szymczak-Graczyk, Solid truss to shell numerical homogenization of prefabricated composite slabs, *Materials*, **14**(15): 4120, 2021, https://doi.org/10.3390/ma14154120.

34. Abaqus Finite Element Analysis, Abaqus Unified FEA® Software, https://www.3ds.com/products-services/simulia/products/abaqus (accessed on 15 July 2024).

35. T. Łodygowski, *Geometrycznie nieliniowa analiza sztywno-plastycznych i sprężysto-plastycznych belek i ram płaskich* [in Polish], IPPT PAN, Warszawa, 1982.

36. T. Łodygowski, M. Szumigała, Engineering models for numerical analysis of composite bending members, *Mechanics of Structures and Machines*, **20**: 363–380, 1992, https://doi.org/10.1080/08905459208905173.

37. M.C. Biggs, Constrained minimization using recursive quadratic programming, *Towards Global Optimization*, **106**: 1–6, 1975.

38. S.P. Han, A globally convergent method for nonlinear programming, *The Journal of Optimization Theory and Applications*, **22**(3): 297–309, 1977.

39. M.J.D. Powell, The convergence of variable metric methods for nonlinearly constrained optimization calculations, [in:] *Proceedings of the Special Interest Group on Mathematical Programming Symposium Conducted by the Computer Sciences Department at the University of Wisconsin–Madison*, July 11–13, Academic Press, Cambridge, MA, USA, 1977, https://doi.org/10.1016/b978-0-12-468660-1.50007-4.

40. M.J.D. Powell, A fast algorithm for nonlinearly constrained optimization calculations, [in:] G.A. Watson [Ed.], *Numerical Analysis. Lecture Notes in Mathematics*, vol. 630, pp. 144–157, Springer, Berlin, Heidelberg, 1978, https://doi.org/10.1007/BFb0067703.

41. J. Nocedal, S.J. Wright, *Numerical Optimization*, 2nd ed., Springer, Berlin/Heidelberg, 2006.

42. C.G. Broyden, The convergence of a class of double-rank minimization algorithms 1. General considerations, *IMA Journal of Applied Mathematics*, **6**(1): 76–90, 1970, https://doi.org/10.1093/imamat/6.1.76.

43. R. Fletcher, A new approach to variable metric algorithms, *The Computer Journal*, **13**(3): 317–322, 1970, https://doi.org/10.1093/comjnl/13.3.317.

44. D. Goldfarb, A family of variable-metric methods derived by variational means, *Mathematics of Computation*, **24**(109): 23–26, 1970, https://doi.org/10.2307/2004873.

45. D.F. Shanno, Conditioning of quasi-Newton methods for function minimization, *Mathematics of Computation*, **24**(111): 647–656, 1970, https://doi.org/10.2307/2004840.

Received December 7, 2024; revised version April 9, 2025; accepted April 25, 2025; published online May 19, 2025.